Transition states near rank-two saddles: Correlated electron dynamics of helium

George Haller [a], T. Uzer [b], Jesús Palacián [c], Patricia Yanguas [c], Charles Jaffé [d],*

[a] Department of Mechanical Engineering, Massachusetts Institute of Technology, Cambridge, MA 02139, USA
[b] Center for Nonlinear Sciences, School of Physics, Georgia Institute of Technology, Atlanta, GA 30332-0430, USA
[c] Departamento de Ingeniería Matemática e Informática, Universidad Pública de Navarra, 31006 Pamplona, Spain
[d] Department of Chemistry, West Virginia University, Morgantown, WV 26506-6045, USA

ARTICLE INFO

ABSTRACT

The phase space structure in the vicinity of a rank-two saddle is explored both analytically and numerically. In particular, the geometry of electron dynamics in the neighborhood of the rank-two saddle associated with the nonsequential double ionization of helium is analyzed. As in the rank-one saddle case, codimension-one normally hyperbolic invariant manifolds turn out to control the rates of the correlated electron dynamics within each energy surface. The construction of these manifolds, however, is more involved here and requires the use of pseudo-hyperbolic invariant manifold theory. Two distinct correlated motions occur, the nonsequential double ionization and the nonsequential exchange of electrons. The relative rates of crossing the barrier are related to the Lyapunov exponents. The dynamics associated with the larger of the two Lyapunov exponents predominates.

© 2009 Elsevier B.V. All rights reserved.

1. Introduction

Correlated motions are observed in the dynamics of virtually all physical systems. The vibrational modes of nuclei within a molecule are one of the most studied examples [1,2]. The description of these dynamics is based upon a normal mode analysis of the dynamics in the vicinity of a minimum of the molecular potential energy surface. This analysis yields a set of dynamical modes that describes the collective motions of nuclei and that are decoupled in the quadratic (harmonic) approximation. This approach will be familiar to all scientists and mathematicians who study the dynamics of mechanical systems in the vicinity of stable equilibrium points.

The correlated dynamics of electrons represents a more difficult problem. A classic example is the mechanism of an organic reaction [3,4]. Typically, these consist of a couple of chemical structures, with a series of arrows showing how the electrons must rearrange in the course of the reaction. Chemical bonds are formed and broken in the process of this collective motion of the electrons [5,6]. Despite valiant efforts, the full complexity of these correlated dynamics are beyond the reach of current quantum mechanical methods.

---

* Corresponding author.
  E-mail address: cjaffe@wvu.edu (C. Jaffé).

Correlated electronic dynamics are also of importance in atomic systems. Of current interest is the double ionization of various atoms (and molecules) in an intense laser field [7]. This example presents a case where correlated electron dynamics can be readily observed and for which theory has had some degree of success. In early studies with less intense lasers, the processes that were observed involve sequential ionizations, that is, a sequence of single-electron events. It has only been in the last couple of decades, with the development of lasers of sufficient intensity, that experimentalists have been able to observe ionization processes involving two and more electrons. Classical-mechanical treatments have found significant interest as they have been able to account for much of the qualitative features of the experiments [7–9]. For example, it was recognized [10–12] (also classically) that the so-called Stark saddle is a rank-two saddle and that it plays a role in the nonsequential double electron ionization which is analogous to (but more complex than the) better-known ionization of hydrogen in an electric field.

This communication builds on these classical ideas of double-ionization, taking Eckhardt and Sacha's model as its starting point [10–12]. First, the Stark saddle is identified. It is observed to belong to the C_{2v} point group. In the immediate vicinity of the saddle point a harmonic approximation is appropriate. A normal mode analysis of the dynamics in the vicinity of the saddle point identifies three stable or elliptical modes and two unstable or hyperbolic modes. These are the normal modes and their symmetry properties are identified.

Our discussion at this point turns to the phase space geometry in the vicinity of the Stark saddle point. First the six-dimensional center manifold of the Stark saddle is identified. It is observed that the center manifold possesses two-dimensional stable and unstable manifolds. Both of these manifolds have a weak (or slow) direction and a strong (or fast) direction. A geometrical structure consisting of the center manifold together with the slow components of both the stable and unstable manifolds is constructed. The intersection of this eight-dimensional object with the energy shell is a seven-dimensional surface that plays a role analogous to the normally hyperbolic invariant manifolds (NHIMs) in the transition state theory developed for rank-one saddles [13–15].

These objects are readily constructed in the harmonic approximation. The question of interest is whether they will continue to exist with the inclusion of higher order terms. As a consequence of the unbounded nature of the NHIM the classic theory of normally hyperbolic invariant manifolds cannot be used to conclude the persistence of the NHIM under the addition of nonlinear terms. This difficulty is surmounted by focusing on the nonlinear continuation of the pseudo-stable and pseudo-unstable subspaces, resulting in a set of conditions under which these surfaces continue to exist. This extends the recently formulated geometric transition state theory [13–15] from rank-one saddles to rank-two saddles. A generalization to saddles of arbitrary rank will appear elsewhere.

In Section 4 some of the more interesting dynamical consequences of this analysis are illustrated using classical trajectories. These and related implications are discussed in Section 5.

2. Helium

Helium is one of the simplest systems in which correlated dynamics can be observed [8,9]. When placed in a strong electric field, it can ionize when an electron escapes over (or through) the Stark barrier. In the nonsequential double ionization of Helium both electrons escape together in such a manner that their dynamics are correlated. This is quite distinct from the more commonly observed multiple-ionization processes that consist of a sequence of single electron events and results with free-electrons that are not correlated.

The nonsequential double ionization is not the only process that involves correlated dynamics. Consider the scattering of a free-electron from a He$^+$ ion. Stark resonances are observed. Here the scattering electron crosses and then is trapped behind the Stark barrier and at some time later one of the electrons escapes. This is a sequence of single electron events and the dynamics of the free electrons before and after the collision are not correlated. Another feasible process consists of the exchange of the two electrons, that is, as the scattering (or free) electron crosses the Stark barrier on its inward journey, the bound electron crosses the Stark barrier on its outward journey. In these circumstances the dynamics of the free electrons, before and after the collision, are correlated.

It is clear from this discussion that the Stark barrier plays an important role in the correlated dynamics of this system.

2.1. Model

The mass of the Helium nucleus is taken to be infinite. The mass of the electrons are taken to be unity. The charge of the nucleus is +2 while the electrons have charge -1. The system has six degrees of freedom. The three degrees of freedom associated with the center of mass are neglected as a direct result of the assumption of the nucleus having infinite mass. The six degrees of freedom describe the two vectors that point from the nucleus to each of the two electrons. The z-axis is defined to be in the direction of the electric field. Each of the vectors describing the positions of the two electrons are represented in cylindrical coordinates, (ρ_1, ϕ_1, z_1) and (ρ_2, ϕ_2, z_2). An additional integral of the motion exists, namely the angular momentum about the z-axis defined by the electric field. Consequently, the problem can be reduced to one of five degrees of freedom, as is standard for the n body problem, see [16,17].

The Hamiltonian is given by:

$$H = \frac{1}{2}\left(P_{\rho_1}^2 + \frac{P_{\phi_1}^2}{\rho_1^2} + P_{z_1}^2\right) + \frac{1}{2}\left(P_{\rho_2}^2 + \frac{P_{\phi_2}^2}{\rho_2^2} + P_{z_2}^2\right) - \mathcal{F}(z_1 + z_2) - \frac{2}{\sqrt{\rho_1^2 + z_1^2}} - \frac{2}{\sqrt{\rho_2^2 + z_2^2}}$$
$$+ \frac{1}{\sqrt{\rho_1^2 + \rho_2^2 - 2\rho_1\rho_2\cos(\phi_1 - \phi_2) + (z_1 - z_2)^2}}. \tag{1}$$

The first two terms are the kinetic energy of the two electrons. The third term represents the interaction of the electrons with the electric field. Here $\mathcal{F}$ is the strength of the field. The fourth and fifth terms are the attractive interactions between the nucleus and the electrons and the last term is the repulsive interaction between the two electrons. It is the last term in this Hamiltonian that gives rise to the correlation between the two electrons. The zero of the energy scale is chosen when the three particles are infinitely separated and at rest.

2.2. The Stark saddle

The immediate goal is to locate and characterize the stationary point at the top of the Stark barrier. First observe that the Stark saddle is in coordinate space and thus $P_{\rho_1} = P_{\rho_2} = P_{\phi_1} = P_{\phi_2} = P_{z_1} = P_{z_2} = 0$. The standard analysis locates the stationary point at $\rho_1 = \rho_2 = \rho_s$, $\phi_1 = \pi/2$, $\phi_2 = -\pi/2$ and $z_1 = z_2 = z_s = \sqrt{3}\rho_s$ and where $\rho_s = 3^{1/4}/(2\sqrt{\mathcal{F}})$. The energy of the saddle is $E_s = -6\sqrt{\mathcal{F}/\sqrt{3}}$. In all numerical examples the electric field strength is taken to be $\mathcal{F} = 0.137$.

Recall that the variables (ρ_i, ϕ_i, z_i) are the components of the vector that connects the nucleus with the ith electron. As a direct consequence of $P_{\phi_1} = P_{\phi_2} = 0$ the dynamics are confined to a vertical plane. While this plane is arbitrary, the choice of $\phi_1 = -\phi_2 = \pi/2$ results in the dynamics being confined to the yz-plane. The equilibrium configuration of the two electrons and the nucleus is shown in Fig. 1. The point group of this equilibrium configuration is C_{2v}.

In order to determine the stability properties of the Stark saddle the Hamiltonian is expanded in a power series about the stationary point to obtain the quadratic approximation,

$$H_2 = \frac{1}{2}P_{\rho_1}^2 + \frac{1}{2}P_{\rho_2}^2 + \frac{1}{2}P_{z_1}^2 + \frac{1}{2}P_{z_2}^2 + \frac{4}{r_s^2}P_{\phi_1}^2 + \frac{1}{2r_s}\phi_1^2 + \frac{5}{4r_s^3}(\rho_1 - \rho_s)^2 + \frac{2}{r_s^3}(\rho_2 - \rho_s)(\rho_1 - \rho_s) + \frac{5}{4r_s^3}(\rho_2 - \rho_s)^2$$
$$- \frac{7}{4r_s^3}(z_1 - z_s)^2 + \frac{1}{r_s^3}(z_1 - z_s)(z_2 - z_s) - \frac{7}{4r_s^3}(z_2 - z_s)^2 + \frac{3}{2r_s^3}\sqrt{3}(\rho_1 - \rho_s)(z_2 - z_s) + \frac{3}{2r_s^3}\sqrt{3}(\rho_2 - \rho_s)(z_1 - z_s) \tag{2}$$

where $r_s = 2\rho_s$. Standard normal mode analysis is used to decouple the dynamical modes. This yields a Hamiltonian of the form

$$H = E_s + \frac{1}{2}\sum_{i=1}^{2}\left(p_i^2 - \lambda_i^2 q_i^2\right) + \frac{1}{2}\sum_{i=3}^{5}\left(p_i^2 + \omega_i^2 q_i^2\right) + f(I_1, I_2, p_3, p_4, p_5, q_3, q_4, q_5), \tag{3}$$
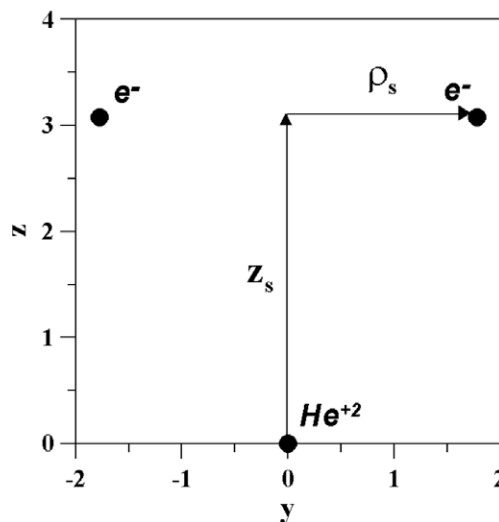

Fig. 1. The coordinate space configuration of the Stark saddle for helium in a strong electric field. The coordinates are chosen such that the Stark saddle lies in the yz-plane; the electric field lies along the z-axis. In the infinite mass limit the nucleus lies at the origin. The stationary point in the Stark saddle is reached when the two electrons are at $(\pm\rho_s, z_s)$. Observe that $\rho_s/z_s = \sqrt{3}$. Consequently, the stationary point consists of the three particles sitting at rest in an equilateral triangle. The area enclosed is proportional to the field strength. This equilibrium configuration belongs to the point group C_{2v}.

where $I_1 = \frac{1}{2}(p_1^2 - \lambda_1^2 q_1^2)$, $I_2 = \frac{1}{2}(p_2^2 - \lambda_2^2 q_2^2)$, and $f(p,q) = \mathcal{O}(q_i^k p_j^l)$, $k + l \geqslant 3$, and where f is a C^{r+1} function with $r \geqslant 1$. In addition note that $0 < \lambda_2 < \lambda_1$. The Lyapunov exponents (λ_i) and normal mode frequencies (ω_i) are given in Table 1. Observe that the Stark saddle is of rank two with two unstable modes while the three remaining are stable. The analysis identifies the irreducible representations which characterize each of the normal modes. Note that both the two unstable modes and the three stable modes are of different symmetry. Trajectories corresponding to the two unstable (hyperbolic) modes are shown in Fig. 2. The totally symmetric A_1 hyperbolic mode is shown in Fig. 2(a) and the antisymmetric B_2 hyperbolic mode is seen in Fig. 2(e). Observe that in both figures the trajectories of the two electrons are mirror images of each other. The difference in the dynamical behavior is in the direction that the electron traverses the trajectory. In the first case (A_1) both electrons travel in the same directions as is indicated by the arrows on the trajectories. In the second case (B_2), the trajectories are time-reversed images of each other and the electrons traverse the trajectories in opposite directions. Again, this is indicated by the arrows on the trajectories.

Clearly, the conjecture that the nature of the correlated dynamics is dependent on the properties of the Stark saddle appears to be correct. The structure imposed upon phase space by the existence of the Stark saddle will be discussed in the next section.

3. Phase space geometry

The structure of phase space in the vicinity of the Stark saddle is discussed in this section. The discussion is broken into two parts. In the first part, the geometry of the linearized Hamiltonian flow is described. In the second, the extension of the geometry to the full nonlinear system is considered. Unlike in the rank-one saddle case, this extension cannot be accomplished through classic normally hyperbolic invariant manifold theory [18]. This is discussed and a method for overcoming this difficulty is presented in the second subsection. The full details of the proof and its generalization to higher rank saddles will be presented elsewhere.

Table 1
The normal mode frequencies and Lyapunov exponents. Shown here are the stabilities, symmetry properties and frequencies (ω_i) of the three stable normal modes and the Lyapunov exponents (λ_i) for the two unstable modes. Here $\mathcal{F}$ is the electric field strength.

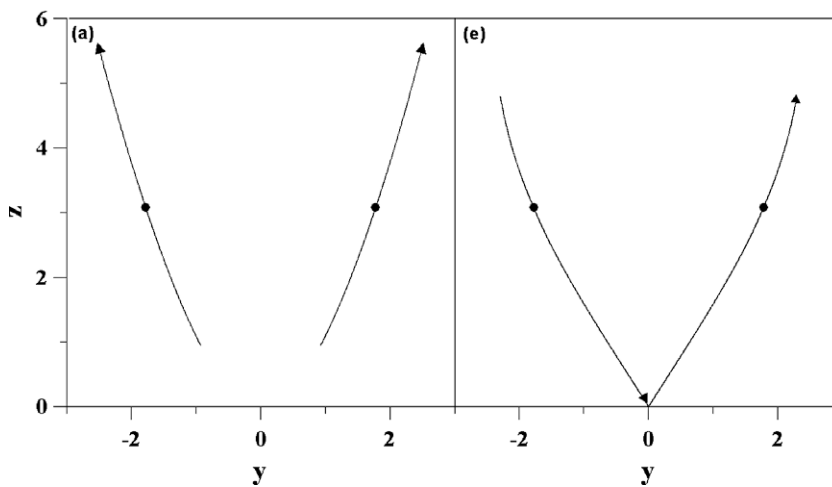| Mode (i)	Stability	Irreducible representation	Frequencies and Lyapunov exponents
1	Unstable	B_2	$\lambda_1 = 1.56815\,\mathcal{F}^{3/4}$
2	Unstable	A_1	$\lambda_2 = 1.21389\,\mathcal{F}^{3/4}$
3	Stable	A_1	$\omega_3 = 1.53327\,\mathcal{F}^{3/4}$
4	Stable	B_2	$\omega_4 = 0.839251\,\mathcal{F}^{3/4}$
5	Stable	B_1	$\omega_5 = 0.936687\,\mathcal{F}^{3/4}$

Fig. 2. The two hyperbolic normal modes. Shown here are two classical trajectories. The one labeled (a) is the symmetric (A_1) hyperbolic mode and that labeled (e) is the antisymmetric (B_2) hyperbolic mode. The initial conditions were chosen so that the two electrons pass through the Stark saddle (the two black Dots) at the same time. It should be noted that the two electron trajectories are mirror images of each other and that for the A_1 hyperbolic mode the electrons traverse the two trajectories in same direction while for the B_2 hyperbolic mode the electrons traverse the two trajectories in the opposite directions. The Lyapunov exponents (λ_1, λ_2) for these two modes are given in Table 1 where it is seen that the antisymmetric mode is the dominant hyperbolic mode.

3.1. Linearized phase space geometry

The linearized Hamiltonian dynamics in the vicinity of the Stark saddle of system (1) is generated by the quadratic Hamiltonian

$$H_2(p,q) = \frac{1}{2} \sum_{i=1}^{2} \left(p_i^2 - \lambda_i^2 q_i^2\right) + \frac{1}{2} \sum_{i=3}^{5} \left(p_i^2 + \omega_i^2 q_i^2\right). \tag{4}$$

The origin $p = 0$, $q = 0$ admits six elliptic directions within the center subspace E^c; rotations within this subspace are governed by the three frequencies ω_i. The origin also has a two-dimensional stable subspace E^s and a two-dimensional unstable subspace E^u. The geometry of the phase space for the Hamiltonian (4) is sketched in Fig. 3. Exponential growth and decay in $E^s \times E^u$ is governed by the Lyapunov exponents

$$-\lambda_1 < -\lambda_2 < 0 < \lambda_2 < \lambda_1. \tag{5}$$

Observe that λ_1 is strictly larger than λ_2 for all values of the electric field $\mathcal{F}$. This will be essential for the linearized geometry to be relevant for the full Hamiltonian H near the origin. The three frequencies and the two Lyapunov exponents are given in Table 1.

Two invariant subspaces within E^s and E^u are defined, respectively, by writing

$$E^s = E_1^s \times E_2^s, \qquad E^u = E_1^u \times E_2^u.$$

Here E_i^s refers to the invariant subspace spanned by the eigenvector corresponding to the exponent $-\lambda_i$; the notation for E_i^u is similar. Refer to E_1^s and E_1^u as the *strong stable subspace* and the *strong unstable subspace* of the origin, respectively.

Define the λ_2-*unstable subspace* of the origin, $E_{\lambda_2}^u$, as the maximal invariant subspace in which the norm of solutions decays no faster than $e^{-\lambda_2 t}$. Note that $E_{\lambda_2}^u$ is a nine-dimensional subspace of the form

$$E_{\lambda_2}^u = E^c \times E_2^s \times E^u. \tag{6}$$

The subspace $E_{\lambda_2}^u$ is often called a *pseudo-unstable subspace*, because it is only unstable relative to the strong stable subspace E_1^s. The geometry of the pseudo-unstable subspace $E_{\lambda_2}^u$ is shown in Fig. 4.

Similarly, define the λ_2-*stable subspace*, $E_{\lambda_2}^s$, as the maximal invariant subspace in which the norm of solutions grows at no faster than $e^{\lambda_2 t}$. Note that $E_{\lambda_2}^s$ is also a nine-dimensional subspace of the form

$$E_{\lambda_2}^s = E^c \times E^s \times E_2^u,$$

often called a *pseudo-stable subspace*. The corresponding geometry is also shown in Fig. 4. Unlike classic stable and unstable subspaces, the pseudo-stable and pseudo-unstable subspaces, $E_{\lambda_2}^s$ and $E_{\lambda_2}^u$, are not disjoint: their intersection is the eight-dimensional subspace

$$C = E_{\lambda_2}^s \cap E_{\lambda_2}^u = E^c \times E_2^s \times E_2^u$$

that contains all center directions as well as the weaker stable and unstable directions.

Consider now the intersections of C with the quadratic energy surface

$$\mathcal{E}_h = \left\{(q,p) \in \mathbb{R}^{10} : H_2(q,p) = h > 0\right\}.$$

This intersection,

$$C_h = \mathcal{E}_h \cap C = \left\{(p,q) \in \mathbb{R}^{10} : \frac{1}{2}\left(p_2^2 - \lambda_2^2 q_2^2\right) + \frac{1}{2} \sum_{i=3}^{5} \left(p_i^2 + \omega_i^2 q_i^2\right) = h > 0, q_1 = 0, p_1 = 0\right\}, \tag{7}$$
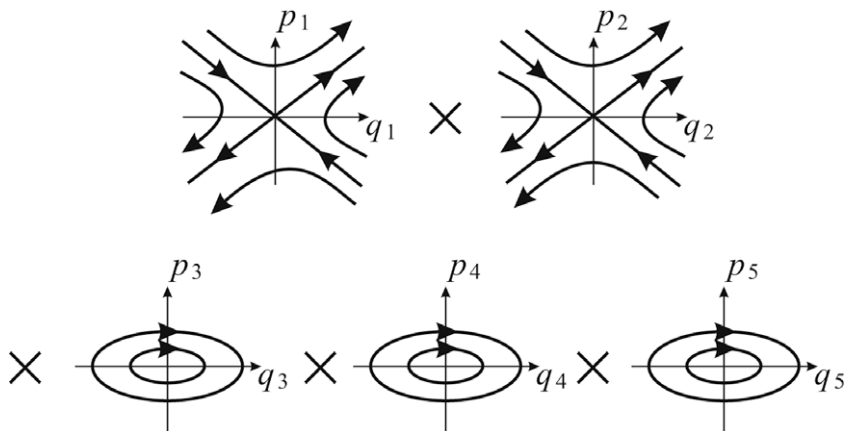

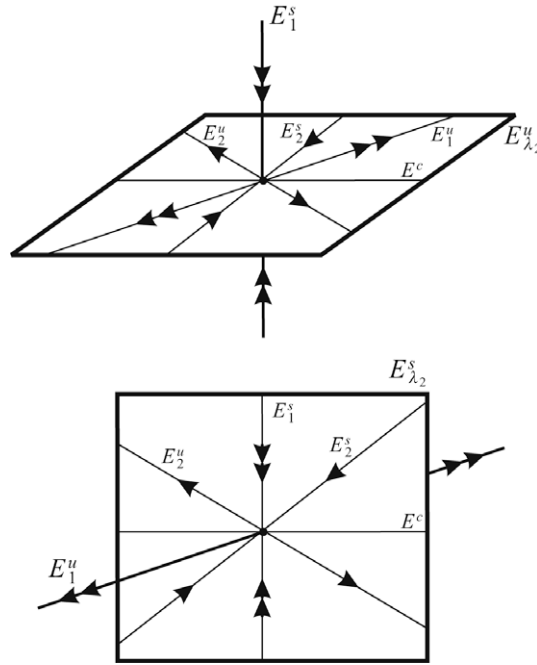**Fig. 3.** Phase space geometry of the Hamiltonian (4).

Fig. 4. Geometry of the pseudo-unstable subspace $E^u_{\lambda_2}$ and of the pseudo-stable subspace $E^s_{\lambda_2}$.

is the analogue of the normally hyperbolic invariant sphere that forms the cornerstone of transition state theory near rank-one saddles [13–15]. The surface C_h is called the *normally hyperbolic invariant manifold* (NHIM). Geometrically, C_h is diffeomorphic to near-critical energy surfaces of a Hamiltonian with a rank-one saddle. Such a near-critical energy surface contains a normally hyperbolic invariant sphere as well as its stable and unstable manifolds.

The surface C_h is a seven-dimensional manifold. It is normally hyperbolic within the energy surface C_h by condition (5). This means that growth and decay rates in directions normal to C_h, but still tangent to the energy surface, dominate growth and decay rates in directions tangent to C_h. Also, C_h has codimension-one (i.e., eight-dimensional) stable and unstable manifolds within the energy surface $\mathcal{E}_h$, given by

$$
\begin{aligned}
W^s(C_h) &= \{(p,q) \in \mathbb{R}^{10} : H_2(p,q) = h > 0, \quad p_1 = -\lambda_1 q_1\}, \\
W^u(C_h) &= \{(p,q) \in \mathbb{R}^{10} : H_2(p,q) = h > 0, \quad p_1 = \lambda_1 q_1\}.
\end{aligned}
\tag{8}
$$

These manifolds can be partitioned into two parts; a forward part and a backward part,

$$
\begin{aligned}
W^s_f(C_h) &= \{(p,q) \in \mathbb{R}^{10} : H_2(p,q) = h > 0, \quad p_1 = -\lambda_1 q_1 \geqslant 0\}, \\
W^u_f(C_h) &= \{(p,q) \in \mathbb{R}^{10} : H_2(p,q) = h > 0, \quad p_1 = \lambda_1 q_1 \geqslant 0\}, \\
W^s_b(C_h) &= \{(p,q) \in \mathbb{R}^{10} : H_2(p,q) = h > 0, \quad p_1 = -\lambda_1 q_1 \leqslant 0\}, \\
W^u_b(C_h) &= \{(p,q) \in \mathbb{R}^{10} : H_2(p,q) = h > 0, \quad p_1 = \lambda_1 q_1 \leqslant 0\}.
\end{aligned}
\tag{9}
$$

The forward and backward parts of these two manifolds join smoothly

$$
\begin{aligned}
W_f(C_h) &= W^s_f(C_h) \cup W^u_f(C_h), \\
W_b(C_h) &= W^s_b(C_h) \cup W^u_b(C_h),
\end{aligned}
$$

to yield two eight-dimensional invariant tubes that, respectively, correspond to the forward and backward reactive tubes. They are embedded in the nine-dimensional energy shell and hence are codimension-one. Consequently, the states within these tubes remain confined to the tubes and flow from the interior of W^s_j into the interior of W^u_j (where $j = f$ or b). It should be noted that the intersection of the forward (backward) tubes is just the NHIM

$$
\begin{aligned}
C_h &= W^s_f(C_h) \cap W^u_f(C_h), \\
C_h &= W^s_b(C_h) \cap W^u_b(C_h).
\end{aligned}
$$

Two transition states can now be defined as cross-section surfaces in each of the forward and backward reactive tubes,

$$TS_f(C_h) = \left\{ (p,q) \in \mathbb{R}^{10} : \frac{1}{2}p_1^2 + \frac{1}{2}(p_2^2 - \lambda_2^2 q_2^2) + \frac{1}{2}\sum_{i=3}^{5}(p_i^2 + \omega_i^2 q_i^2) = h > 0, q_1 = 0, p_1 \geqslant 0 \right\},$$

$$TS_b(C_h) = \left\{ (p,q) \in \mathbb{R}^{10} : \frac{1}{2}p_1^2 + \frac{1}{2}(p_2^2 - \lambda_2^2 q_2^2) + \frac{1}{2}\sum_{i=3}^{5}(p_i^2 + \omega_i^2 q_i^2) = h > 0, q_1 = 0, p_1 \leqslant 0 \right\}.$$

These are, respectively, the forward and backward transition states. Their union is an eight-dimensional unbounded surface and their intersection is simply the NHIM, C_h. And finally, we observe that all states exterior to the two reactive tubes do not react, that is, they are confined to either reactant or product regions of phase space for all time.

3.2. Full phase space geometry

The next goal is to extend the geometry described above for the linearized Hamiltonian flow to the full nonlinear system. Unlike in the rank-one saddle case, this extension cannot be accomplished through classic normally hyperbolic invariant manifold theory [18]. The reason for this is the unboundedness of the set C_h.

The classic theory of normally hyperbolic invariant manifolds only applies to compact manifolds such as spheres. This is not just a technicality: unbounded invariant manifolds will, in general, not persist under the addition of the nonlinear terms. Hence, there is no immediately applicable result that would guarantee the nonlinear continuation of the noncompact set C_h or of its stable and unstable manifolds.

To circumvent this problem, we focus on the nonlinear continuation of the pseudo-stable and pseudo-unstable subspaces, $E_{\lambda_2}^s$ and $E_{\lambda_2}^u$. The continuation turns out to exist under condition (5): we refer to a nonlinear continuation of $E_{\lambda_2}^s$ as a *pseudo-stable manifold* $W^{ps}(0)$ of the origin; a nonlinear continuation of $E_{\lambda_2}^u$ is called a *pseudo-unstable manifold* $W^{pu}(0)$ of the origin. We sketch the geometry of the pseudo-unstable manifold in Fig. 5.

The manifolds $W^{ps}(0)$ and $W^{pu}(0)$ are invariant, but they do not have the properties of classical stable and unstable manifolds. They are not unique and they are not as smooth as the Hamiltonian flow map

$$\mathcal{F}^t : \mathbb{R}^{10} \to \mathbb{R}^{10},$$
$$(p_0, q_0) \mapsto (p(t), q(t)).$$

Furthermore, most solutions in $W^{ps}(0)$ do not tend to the origin in forward time, and most solutions in $W^{pu}(0)$ do not tend to the origin in backward time. Solutions in $W^{ps}(0)$, however, can only grow at speeds slightly above $e^{\lambda_2 t}$ while they are close to the origin. Likewise, solutions in $W^{pu}(0)$ can only grow in backward time at speeds slightly above $e^{\lambda_2 t}$ while they are in the vicinity of the origin. Finally, both manifolds are nine-dimensional invariant surfaces and hence locally divide the full 10-dimensional phase space (cf. [19,20]). The following theorem summarizes these properties of the pseudo-stable and pseudo-unstable manifolds.

Theorem 1. *Assume that condition (5) holds, and define the constant*

$$\bar{r} = \min\left(\text{Int}[\lambda_1/\lambda_2], r\right), \tag{10}$$

with Int[·] referring to the integer part of a number; recall that $r \geqslant 1$ is the degree of smoothness for the Hamiltonian H defined in (3). Then the $q = p = 0$ fixed point of the full Hamiltonian H admits a (nonunique) nine-dimensional class $C^{\bar{r}}$ pseudo-stable manifold $W^{ps}(0)$ and a (nonunique) nine-dimensional class $C^{\bar{r}}$ pseudo-unstable manifold $W^{pu}(0)$; these manifolds are tangent to the subspaces $E_{\lambda_2}^s$ and $E_{\lambda_2}^u$, respectively, at the origin.

If the function $f(p,q)$ is small enough globally in the $C^{\bar{r}+1}$ norm (which can always be achieved by smoothly deforming the Hamiltonian outside a small enough neighborhood of the origin), then for the constant

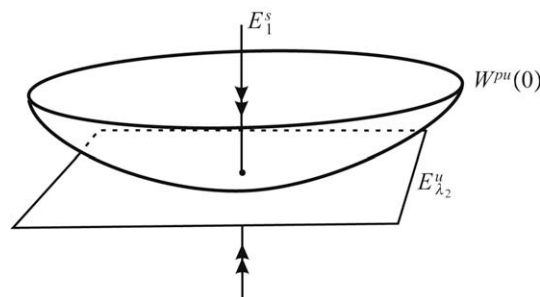$$a = \exp\left[(\lambda_2 + \lambda_1/\text{Int}[\lambda_1/\lambda_2])/2\right],$$

Fig. 5. The geometry of the pseudo-unstable manifold $W^{pu}(0)$.

we have

$$W^{ps}(0) = \left\{ (p,q) \in \mathbb{R}^{10} : \sup_{t \geqslant 0} |\mathcal{F}^t(p,q)| a^{-t} < \infty \right\}, \tag{11}$$

i.e., $W^{ps}(0)$ consists of solutions that grow at most at the rate a^t. Similarly,

$$W^{pu}(0) = \left\{ (p,q) \in \mathbb{R}^{10} : \sup_{t \leqslant 0} |\mathcal{F}^t(p,q)| a^{-t} < \infty \right\}. \tag{12}$$

Proof. The theorem can be proved by applying Irwin's theorem [19,20] on pseudo-stable manifolds in the current context. We spell out the details for $W^{ps}(0)$; the proof being identical for $W^{pu}(0)$ in backward time.

First, note that $E^s_{\lambda_2} \oplus E^u_1$ is an invariant splitting for the linearized time-one map $D\mathcal{F}^t(0)$. The estimates

$$\left\| D\mathcal{F}^t(0) \right\|_{E^s_{\lambda_2}} = e^{\lambda_2} < a, \tag{13}$$

and

$$\left\| D\mathcal{F}^t(0) \right\|^{-1}_{E^u_1} = e^{-\lambda_1} < a^{-\rho} \tag{14}$$

hold simultaneously for some constant $a > 0$ and integer $\rho \geqslant 1$, whenever

$$e^{\lambda_2} < a < e^{\lambda_1/\rho}. \tag{15}$$

Such a constant $a > 0$ always exists if we select

$$\rho = \mathrm{Int}[\lambda_1/\lambda_2]. \tag{16}$$

In that case, the choice of

$$a = \exp\left[(\lambda_2 + \lambda_1/\mathrm{Int}[\lambda_1/\lambda_2])/2 \right] \tag{17}$$

ensures that (15) holds.

Conditions (13) and (14) are precisely the two main conditions of Irwin's theorem in [19]. As a result, whenever (16) holds, Irwin's theorem guarantees the existence of a (non-unique) class-C^ρ pseudo-stable invariant manifold $W^{ps}(0)$ that is tangent to the subspace $E^s_{\lambda_2}$ at the origin. To be precise, the degree $\bar{r}$ of smoothness of $W^{ps}(0)$ is the minimum of r, the smoothness of the time-one map, and of ρ, which gives the expression (10). The characterization (11) of the pseudo-stable manifold follows from general expressions in [19,20] after we set a as in (17). □

Based on the above result, under conditions (5) and (10), codimension-one pseudo-stable and pseudo-unstable invariant manifolds exist at the origin of the phase space. They intersect any nearby energy surface $\mathcal{E}_h$ transversely in the isoenergetic surfaces

$$W^{ps}_h = W^{ps}(0) \cap \mathcal{E}_h, \qquad W^{pu}_h = W^{pu}(0) \cap \mathcal{E}_h,$$

that are codimension-one within $\mathcal{E}_h$.

For any $h > 0$ small enough, the intersection

$$\widetilde{C}_h = W^{ps}_h \cap W^{pu}_h$$

is a smooth continuation of the surface C_h defined in (7). This is the case because W^{ps}_h and W^{pu}_h are smooth perturbations of $E^s_{\lambda_2}$ and $E^s_{\lambda_2}$ near the origin, and the latter two surfaces intersect transversely; hence their intersection smoothly perturbs under small enough perturbations. We conclude that $\widetilde{C}_h$ is diffeomorphic to near-critical energy surfaces of a nine-degree-of-freedom Hamiltonian with a rank-one saddle.

It should also be noted that $\widetilde{C}_h$ is a $\bar{r}$ times continuously differentiable manifold, as it is the transverse intersection of two manifolds of the same degree of smoothness. Since the Hamiltonian is of class C^r for any positive r, the real limitation on $\bar{r}$ is the ratio of the two Lyapunov exponents, λ_1 and λ_2. A Taylor expansion for $\widetilde{C}_h$ near the origin is only guaranteed to exist up to order $\bar{r}$. In the application considered here, $\bar{r} = 1$, since $\mathrm{Int}[\lambda_1/\lambda_2] = 1$ (cf. Table 1).

The stable manifold of $\widetilde{C}_h$ is given by

$$W^s\left(\widetilde{C}_h\right) = W^{ps}_h,$$

a codimension-one surface within the energy surface $\mathcal{E}_h$. Similarly, the unstable manifold of $\widetilde{C}_h$,

$$W^u\left(\widetilde{C}_h\right) = W^{pu}_h,$$

is a codimension-one surface within $\mathcal{E}_h$.

The manifolds $W^s\left(\widetilde{C}_h\right)$ and $W^u\left(\widetilde{C}_h\right)$ will be small deformations of their linearized counterparts, $W^s(C_h)$ and $W^u(C_h)$ (see Eq. (9)).

These manifolds can be partitioned into two parts; a forward part and a backward part,

$$
\begin{aligned}
W_f^s\left(\widetilde{C}_h\right) &= \left\{(p,q)\in\mathbb{R}^{10} : H(p,q)=h>0, \quad p_1=-\lambda_1 q_1 \geqslant 0\right\}, \\
W_f^u\left(\widetilde{C}_h\right) &= \left\{(p,q)\in\mathbb{R}^{10} : H(p,q)=h>0, \quad p_1=\lambda_1 q_1 \geqslant 0\right\}, \\
W_b^s\left(\widetilde{C}_h\right) &= \left\{(p,q)\in\mathbb{R}^{10} : H(p,q)=h>0, \quad p_1=-\lambda_1 q_1 \leqslant 0\right\}, \\
W_b^u\left(\widetilde{C}_h\right) &= \left\{(p,q)\in\mathbb{R}^{10} : H(p,q)=h>0, \quad p_1=\lambda_1 q_1 \leqslant 0\right\}.
\end{aligned}
\tag{18}
$$

The forward and backward parts of these two manifolds join smoothly

$$
\begin{aligned}
W_f\left(\widetilde{C}_h\right) &= W_f^s\left(\widetilde{C}_h\right) \cup W_f^u\left(\widetilde{C}_h\right), \\
W_b\left(\widetilde{C}_h\right) &= W_b^s\left(\widetilde{C}_h\right) \cup W_b^u\left(\widetilde{C}_h\right),
\end{aligned}
$$

to yield two eight-dimensional invariant tubes that, respectively, correspond to the forward and backward reactive tubes. They are embedded in the nine-dimensional energy shell and hence are codimension-one. Consequently, the states within these tubes remain confined to the tubes and flow from the interior of W_j^s into the interior of W_j^u (where $j = f$ or b). It should be noted that the intersection of the forward (backward) tubes is just the NHIM

$$
\begin{aligned}
\widetilde{C}_h &= W_f^s\left(\widetilde{C}_h\right) \cap W_f^u\left(\widetilde{C}_h\right), \\
\widetilde{C}_h &= W_b^s\left(\widetilde{C}_h\right) \cap W_b^u\left(\widetilde{C}_h\right).
\end{aligned}
$$

Two transition states can now be defined as cross-section surfaces in each of the forward and backward reactive tubes,

$$
TS_f\left(\widetilde{C}_h\right) = \left\{(p,q)\in\mathbb{R}^{10} : \frac{1}{2}p_1^2 + \frac{1}{2}(p_2^2 - \lambda_2^2 q_2^2) + \frac{1}{2}\sum_{i=3}^{5}(p_i^2 + \omega_i^2 q_i^2) + f(I_1,I_2,p_3,p_4,p_5,q_3,q_4,q_5) = h>0, q_1=0, p_1 \geqslant 0\right\},
$$

$$
TS_b\left(\widetilde{C}_h\right) = \left\{(p,q)\in\mathbb{R}^{10} : \frac{1}{2}p_1^2 + \frac{1}{2}(p_2^2 - \lambda_2^2 q_2^2) + \frac{1}{2}\sum_{i=3}^{5}(p_i^2 + \omega_i^2 q_i^2) + f(I_1,I_2,p_3,p_4,p_5,q_3,q_4,q_5) = h>0, q_1=0, p_1 \leqslant 0\right\}.
$$

These are, respectively, the forward and backward transition states. Their union is an eight-dimensional unbounded surface and their intersection is simply the NHIM, $\widetilde{C}_h$. And finally, we observe that all states exterior to the two reactive tubes do not react, that is, they are confined to either reactant or product regions of phase space for all time.

The main differences between $W^s\left(\widetilde{C}_h\right)$ and the stable manifold of a NHIM in the rank-one-saddle case are:

- The manifold $W^s\left(\widetilde{C}_h\right)$ is constructed as a pseudo-stable manifold, and hence it is non-unique. However, it is tangent to the unique pseudo-stable subspace, $E_{\lambda_2}^s$, and hence its Taylor expansion is unique up to order $\bar{r}$.
- The manifold $W^s\left(\widetilde{C}_h\right)$ is only of class $C^{\bar{r}}$.
- Typical solutions in $W^s\left(\widetilde{C}_h\right)$ do not tend to $\widetilde{C}_h$ in forward time, but cannot leave $\widetilde{C}_h$ at rates faster than $\exp[t(\lambda_2 + \lambda_1/\mathrm{Int}[\lambda_1/\lambda_2])/2]$ while near $\widetilde{C}_h$.

Similar comments can be made for $W^u\left(\widetilde{C}_h\right)$.

4. Numerical results

The trajectory study presented in the following discussion is intended to illustrate the nature of the competition between the two unstable modes. This is not merely of mathematical interest as the results have significant implications for systems of physical interest. They also provide a clear explanation of the well known generic behavior, long observed, in classical trajectory studies of the simplest planetary model of helium, where one of the electrons escapes to infinity while the second electron dives into the Coulomb singularity.

Consider the classical trajectories shown in Fig. 2. The figure labeled (a) shows the pure symmetric A_1 hyperbolic mode and while that labeled (e) shows the pure antisymmetric B_2 hyperbolic mode. In each of these figures the trajectories of both of the electrons are shown. The initial conditions were chosen as follows: First, each trajectory was started above the stationary point. This leaves only the momenta to be specified. All of the momenta, with the exception of the momentum associated with the mode of interest, are set to zero. This last momentum is chosen so that energy of the system is 0.025 hartrees above the Stark saddle. The sign of this momentum is taken to be positive and the trajectory on either side of the stationary

point is found by integrating Hamilton's equations of motion both forward and backward in time. It should be noted that since the equations of motion are symmetric with respect to time-reversal, each of these figures corresponds one of a pair of trajectories, the second trajectory being obtained by changing the directional arrows on each of the trajectories.

Each of these figures show the trajectories of the electrons in the physical space. The initial conditions were chosen so that the dynamics are confined to the *yz*-plane. This can be done without disrupting the generality of the results. In both cases the electron trajectories pass through the solid dots at the same time. As they pass through these dots they are crossing the Stark saddle. It should be noted that for both the A_1 and the B_2 hyperbolic modes each of the two electron trajectories are mirror images of each other. The difference being that for the A_1 hyperbolic mode the two electrons traverse the trajectory in the same direction, while in the other, that is, the B_2 hyperbolic mode, the two electrons traverse their respective paths in the opposite direction.

Of particular interest is the observation that for the symmetric A_1 mode the two electrons emerge from the classical Coulomb singularity and, after crossing the Stark saddle, both escape to infinity. For the antisymmetric B_2 mode one electron escapes from the classical Coulomb singularity while the second electron approaches the He$^+$ ion from infinity. After both electrons cross the Stark saddle, the one that emerged from the Coulomb singularity escapes to infinity while the second electron, which has been captured, dives into the Coulomb singularity. This second behavior is precisely the generic behavior that has long been observed in classical trajectory studies of helium.

The Lyapunov exponents of these two modes are given in Table 1. Note that the B_2 hyperbolic mode is faster than the A_1 hyperbolic mode. Thus in the analysis of the last section, the first mode (p_1, q_1) corresponds to the B_2 hyperbolic mode and the second mode (p_2, q_2) corresponds to the A_1 hyperbolic mode. This ordering of the Lyapunov exponents is of major significance. As a direct consequence in mixed dynamics, that is when the energy is partitioned between the two hyperbolic modes, while initially the dynamics may resemble the slower A_1 hyperbolic mode, in the long term, it is guaranteed that the dynamics will resemble those of the B_2 hyperbolic mode. In other word, provided that the dynamics have a component in the B_2 hyperbolic direction, in the infinite time limit one of the electrons will escape to infinity while the second dived into the classical Coulomb singularity.

Two additional trajectories are shown in Fig. 6. The initial conditions for these two trajectories are identical to those above with the exception that the energy is now partitioned equally between the two hyperbolic modes, rather than placed in either one or the other. First observe that there are two distinct ways that the energy can be partitioned equally between the two modes. The figure labeled (c) shows one of these and the labeled (g) shows the other. These two figures are simply mirror images of each other. Also note that both of these trajectories also have time-reversed partners. A second observation of interest is that within either figure the two electron trajectories are no longer symmetric. The symmetry in the previous case (see Fig. 2) was due to the fact that they were pure modes and thus mixing the modes destroyed the symmetry. And finally the most important observation is that in the long-time limit the dynamics resembles the B_2 hyperbolic mode in that one electron escapes and the second dives into the Coulomb singularity.

Two more trajectories, labeled (h) and (f) are shown in Fig. 7. The initial conditions for these trajectories are the same as those above with the exception that for the first the energy is partitioned 25%/75% between the A_1 and B_2 hyperbolic modes while in the second the partitioning is reversed at 75%/25%. Both of these have mirror images, which are labeled (b) and (d), and time-reversed pairs. Consider the trajectory labeled (f) first. The behavior here is similar to that seen in the previous two
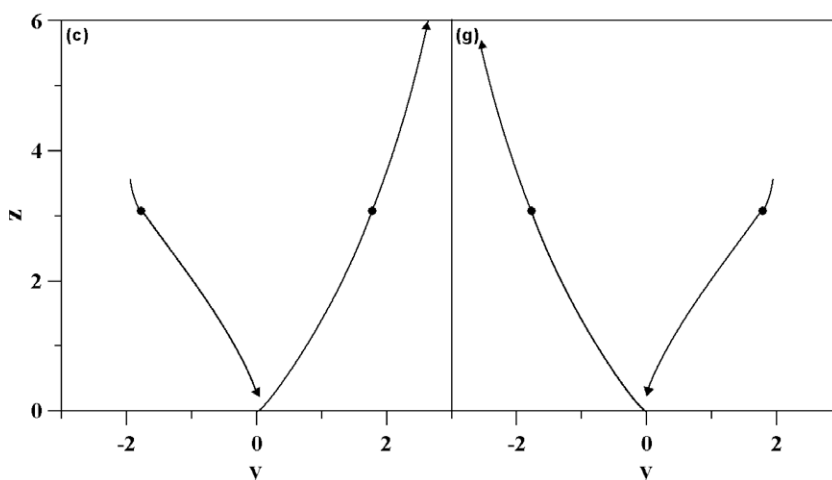

Fig. 6. Two trajectories, labeled (c) and (g), exhibiting mixed hyperbolic mode dynamics. The initial conditions for these trajectories were chosen to ensure that both electrons cross the Stark saddle (the two black dots) at the same time. Additionally, the energy is partitioned equally between the A_1 and the B_2 hyperbolic modes. Note that the symmetry between the two electron trajectories that was observed in Fig. 2 is not present. This symmetry is characteristic of the pure mode dynamics. However, observe that these two examples, (c) and (g), are mirror images of each other. The mixed hyperbolic trajectories always occur as pair of mirror images. Observe that in the long-time limit the dynamics associated with the B_2 hyperbolic mode dominates.
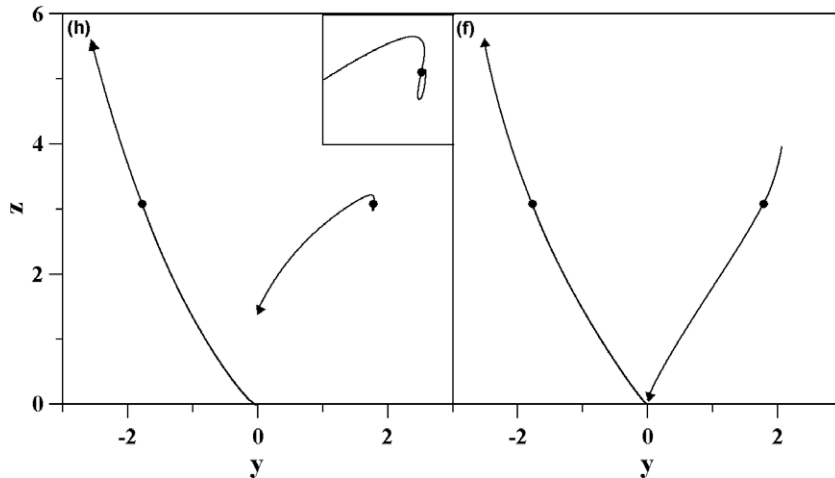
Fig. 7. Two additional trajectories, labeled (h) and (f), exhibiting mixed hyperbolic mode dynamics. The initial conditions for these trajectories were chosen to ensure that both electrons cross the Stark saddle (the two black dots) at the same time. Additionally, for (h) the energy was partitioned 75%/25% between the A_1 and the B_2 hyperbolic modes. For (f) the partitioned of the energy between the A_1 and the B_2 hyperbolic modes was 25%/75%. Of particular interest is the dynamical behavior observed in (h) in the vicinity of the Stark saddle. An expansion of the one electron trajectory on the right-hand side is shown in the inset. Observe that the two electrons will leave the Stark saddle in the same direction, but that in the long-time limit the antisymmetric dynamics of the B_2 hyperbolic mode dominates.

examples (see Fig. 6). This is as expected. The second case, labeled (h), shows more interesting behavior. In this case, in which the majority of the energy has been placed in the symmetric A_1 hyperbolic mode, the initial behavior resembles the pure A_1 mode. Initially both electrons leave the Stark saddle in the same direction (see inset in figure (h) in Fig. 7). It is only at longer times that, after some complicated dynamics, that the dynamics takes on the expected behavior, that is, one electron escaping to infinity while the second electron dives into the Coulomb singularity.

In order to compare these eight trajectories (labeled (a)–(h)) directly, they are plotted in the $q_1 q_2$ coordinate plane, see Fig. 8. Shown here are the eight trajectories discussed in the paragraphs above. They are labeled (a)–(h). The trajectories labeled (a) and (e) are the pure modes and are seen as the heavier lines in Fig. 8. Note that the A_1 hyperbolic mode lies on the q_2 axis and the B_2 hyperbolic mode lies on the q_1 axis. The deviation from the axis, which is most easily seen in the B_2 hyperbolic mode, is due to the breakdown of the harmonic approximation as one leaves the vicinity of the stationary point. The mixed
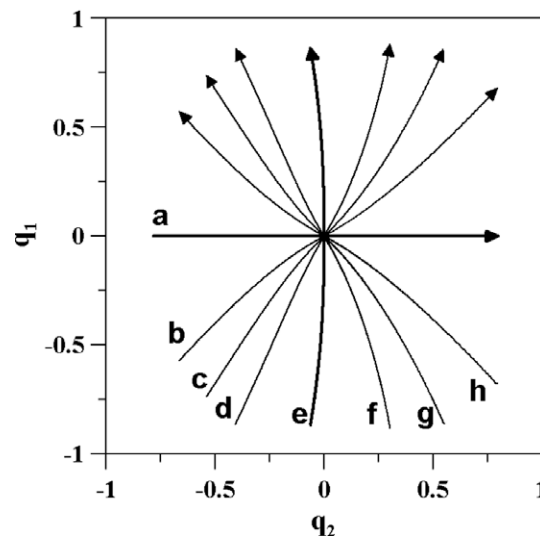

Fig. 8. The hyperbolic coordinate space. In order to compare the trajectories discussed above visually, they are graphed here in the coordinate space defined by the two hyperbolic normal modes. The two dark curves, labeled (a) and (e), are the two pure mode trajectories. The horizontal trajectory, (a), is the pure symmetric (A_1) hyperbolic mode and the vertical trajectory, (e), is the pure antisymmetric (B_2) hyperbolic mode. The curvature observable in antisymmetric trajectory is due to the anharmonic terms in the Hamiltonian. The remaining trajectories are mixed mode trajectories. In each example it is seen that in the long-time limit the B_2 hyperbolic dynamics predominate.

mode trajectories, which are labeled (b), (c), (d), (f), (g), and (h), are also shown. The distance between the system and the q_2 axis is proportional to $e^{\lambda_1 t}$ while the distance between the system and the q_1 axis is proportional to $e^{\lambda_2 t}$. The observed behavior, that is, that in long-time limit one electron escapes to infinity while the second dives into the Coulomb singularity, is a direct consequence of this ordering of the Lyapunov exponents, $\lambda_1 > \lambda_2$.

5. Summary

In this communication we investigate the dynamical behavior in the vicinity of a rank-two saddle in a physical example of current experimental interest. The central result is the proof of the existence of certain geometrical structures (NHIMs, reactive tubes, transition states, etc.) in the vicinity of the rank-two saddle. These structures guide the dynamics across the saddle.

The analysis begins with a simple normal mode analysis of the linearized dynamics in the vicinity of the saddle point. This characterizes the symmetry properties of the two dynamical modes that cross the saddle. In addition it also identifies the rate of crossing of the two modes. This is an important result as one expects the faster of the two modes to dominate the infinite time limit.

The analysis then examines the linearized dynamics in the vicinity of the saddle to define certain geometrical objects. These include the normally invariant manifold C_h, the forward and backward reactive tubes $W_f(C_h)$, $W_b(C_h)$, and the transition states $TS_f(C_h)$, $TS_b(C_h)$. The continued existence of these structures following the introduction of the nonlinearity is the subject of the proof in the third section. These results are then illustrated by a numerical trajectory study.

References

[1] Wilson EB, Decius JC, Cross PC. Molecular vibrations: the theory of infrared and Raman vibrational spectra. New York: McGraw-Hill; 1955.
[2] Orchin M, Jaffé HH. Symmetry, orbitals and spectra. New York: Wiley; 1971.
[3] Woodward RB, Hoffmann R. The conservation of orbital symmetry. Angew Chem Int Ed Engl 1969;8:781–853.
[4] Fukui K. The role of frontier orbitals in chemical reactions (nobel lecture). Angew Chem Int Ed Engl 1982;21:801–9.
[5] Zimmerman H. Möbius–Hückel concept in organic chemistry. Application of organic molecules and reactions. Acc Chem Res 1971;4:272–80.
[6] Dewar MJS. Aromatizität and pericyclische Reaktionen. Angew Chem 1971;83:859–75.
[7] Ho PJ, Panfili R, Haan SL, Eberly JH. Nonsequential double ionization as a completely classical photoelectric effect. Phys Rev Lett 2005;94:093002.
[8] Richter K, Tanner G, Wintgen D. Classical mechanics of two-electron atoms. Phys Rev A 1993;48:4182–96.
[9] Tanner G, Richter K, Rost J-M. The theory of two-electron atoms: between ground state and complete fragmentation. Rev Mod Phys 2000;72:497–544.
[10] Eckhardt B, Sacha K. Wannier threshold law for two-electron escape in the presence of an external electric field. Europhys Lett 2001;56:651–7.
[11] Sacha K, Eckhardt B. Pathways to double ionization of atoms in strong fields. Phys Rev A 2001;63:043414.
[12] Eckhardt B, Sacha K. Classical threshold behavior in a (1 + 1)-dimensional model for double ionization in strong fields. J Phys B 2006;39:3865–71.
[13] Wiggins S, Wiesenfeld L, Jaffé C, Uzer T. Impenetrable barriers in phase-space. Phys Rev Lett 2001;86:5478–81.
[14] Uzer T, Jaffé C, Palacián J, Yanguas P, Wiggins S. The geometry of reaction dynamics. Nonlinearity 2002;15:957–92.
[15] Jaffé C, Kawai S, Palacián J, Yanguas P, Uzer T. A new look at the transition state: Wigner's dynamical perspective revisited. Adv Chem Phys 2005;130A:171–216.
[16] Laub A, Meyer K. Canonical forms for symplectic and Hamiltonian matrices. Celestial Mech 1974;9:213–38.
[17] Meyer KR, Hall G. The introduction to Hamiltonian dynamical systems and the n-body problem. Texts in applied mathematics science. Berlin: Springer; 1992.
[18] Fenichel N. Persistence and smoothness of invariant manifolds for flows. Indiana Univ Math J 1971;21:193–226.
[19] Irwin MC. A new proof of the pseudo-stable manifold theorem. J Lond Math Soc 1980;21:557–66.
[20] de la Llave R, Wayne CE. On Irwin's proof of the pseudo-stable manifold theorem. Mat Z 1995;219:301–21.